Medium Voltage Converter Inductor Insulation Design Considering Grid Requirements

Haiguo Li, *Graduate Student Member, IEEE*, Pengfei Yao, *Member, IEEE*, Zihan Gao, *Student Member, IEEE*, and Fei Wang, *Fellow, IEEE*

***Abstract*— Medium voltage (MV) SiC devices facilitate direct (without 50-/60-Hz transformer) connection of the power electronics converter to the MV grid using simple topology. Compared to the insulation design of MV inductors that have been widely used in the power system, the insulation design of the MV converter filter inductors has new challenges. Particularly, the grid impact on insulation requirements on converter filter inductors is rarely discussed. This article introduces the insulation design of a grid-side filter inductor for a 13.8-kV power conditioning system converter. The grid insulation requirements, including the short-duration power frequency overvoltage and the lightning impulse voltage, are considered in the design. To meet the requirements, the layer-to-layer insulation, winding-to-core/ground insulation, the air gap discharge between the winding and the core, the local electric field, as well as the inter-turn transient voltage distribution are considered. The designed inductors are validated by the 46 kV (>1 min) dc hi-pot test, 12-kV ac partial discharge test, one-hour single-phase converter full rating test, as well as three-phase converter full rating test.**

***Index Terms*— Grid insulation requirements, insulation design, medium voltage (MV) inductor, partial discharge (PD), shielding.**

I. Introduction

WITH medium voltage (MV) SiC devices, power electronics converters can be directly (without 50-/60-Hz transformer) connected to the MV grid with simple topologies [1]. Nevertheless, the direct grid connection exposes the converter to the MV grid and its transients, such as temporary overvoltage and lightning surge. As a result, the converter grid-side filter inductor design needs to consider the grid insulation requirements, including the temporary power frequency overvoltage and the transient lightning and switching overvoltage [2].

Although MV inductors have been widely used in the power system, they are large and heavy because of their high-power ratings. Besides, these inductors are mostly designed with either air core or silicone steel core and only need to consider the fundamental current. However, the converter inductor current consists of high-frequency switching ripples, caused by the high-frequency switching of the power electronics devices, which induce additional winding and core losses, and need to be considered in the inductor design. To improve the converter power density and grid support functions, high switching frequencies are adopted in SiC-based converters thanks to the low switching loss of SiC devices. It is desirable to design a small inductor to fully utilize the benefits of SiC devices. Yet, the insulation requirements, considering the grid-side requirements and the converter-side high voltage (HV), high frequency, and high dv/dt, become a limitation for the inductor power density, and the smaller size means less space for insulation and cooling. Therefore, to reduce the inductor size (potentially cost) and improve the power density, new insulation technology, and/or structure need to be adopted.

There have been some works discussing the MV converter inductor and dc/dc transformer insulation design, and they can be divided into two categories based on their insulation methods.

One method is based on the insulation layers and air gap clearance, which is easy to implement but limited to relatively lower voltage due to the lower insulation capability of air gaps. In [3] and [4], several inductors are connected in series to achieve the HV operation conditions, and insulation layers (Nomex insulation paper, Kapton tape, and customized bobbin) are utilized between the windings and the core to achieve the insulation capability for each inductor. In [5], a bobbin made of insulation material has been used for the insulation between winding and core, and an air gap clearance was used to provide insulation between winding layers.

The other method is based on casting with molds or encapsulation with containers, which is relatively difficult to implement but can be used at a higher voltage level thanks to the better insulation capability of the casting or encapsulant material over the air. In [6], the transformer windings are encapsulated in the 3-D-printed winding package with silicone,

Manuscript received September 17, 2021; revised November 18, 2021; accepted November 24, 2021. Date of publication November 30, 2021; date of current version April 4, 2022. This work was supported primarily by the Advanced Manufacturing Office (AMO), United States Department of Energy, under Award no. DE-EE0008410. This work also made use of the shared facilities of the Engineering Research Center Program of the National Science Foundation and the Department of Energy under NSF Award no. EEC-1041877 and the CURENT Industry Partnership Program. Recommended for publication by Associate Editor Yuko Hirase. *(Corresponding author: Haiguo Li.)*

Haiguo Li and Zihan Gao are with the Department of Electrical Engineering and Computer Science, The University of Tennessee, Knoxville, Knoxville, TN 37996 USA (e-mail: hli96@vols.utk.edu; zgao15@vols.utk.edu).

Pengfei Yao was with the Department of Electrical Engineering and Computer Science, The University of Tennessee, Knoxville, Knoxville, TN 37996 USA. He is now with the China Huaneng Group, Beijing 100031, China (e-mail: yaopf19921210@163.com).

Fei Wang is with the Department of Electrical Engineering and Computer Science, The University of Tennessee, Knoxville, Knoxville, TN 37996 USA, and also with the Oak Ridge National Laboratory, Oak Ridge, TN 37830 USA (e-mail: fred.wang@utk.edu).

Color versions of one or more figures in this article are available at https://doi.org/10.1109/JESTPE.2021.3131602.

Digital Object Identifier 10.1109/JESTPE.2021.3131602

and spacers are used to keep the distance between the winding package and the core. In [7], the winding has been immersed in single-component impregnating at first and then covered with a semiconductive tape to get a smooth electric field, followed by another double-component vacuum casting. Nevertheless, the grid requirements with respect to temporary and transient overvoltage conditions, which can pose more stress on insulation are rarely considered in previous work.

In [8], the grid insulation requirements are considered in the insulation design of a dc/dc transformer operating up to 50 kV. The two windings are vacuum cast in separate molds with epoxy resin, and the designed transformer passes the 70-kV root mean square (rms) (>1 min) ac power frequency test, 35-kV rms partial discharge (PD) test, and 151-kV lightning impulse test. However, the air gaps between two windings and between the winding and the core are sized to avoid PD, which greatly increases the overall size. In [9], the MV-side winding of a dc/dc transformer in a 13.8-kV converter is also cast in molds first with epoxy and then covered by a semiconductive shield, which is grounded, to stress confine the high electrical stress in the insulation material. It passes the 95-kV impulse test, but the PD performances, ac short duration power frequency test, and insulation performances in the converter full voltage rating operation are not provided.

In this article, the insulation design of an ac filter inductor for a 13.8-kV cascaded H-bridge (CHB)-based grid-connected converter is discussed, considering grid insulation requirements. A new insulation structure with the surface conductive shielding is introduced to stress the winding-to-ground potential on the insulation material and avoid PD in the air gaps between the winding and the core. Consequently, the air gaps between the winding and the core/ground can be reduced, and the inductor size can be significantly reduced.

This article is an extension of [10], in which the first and second versions of the inductor design are discussed. However, some thermal issues are found in the second version of the inductor design during further full rating tests. In this article, an improved design, i.e., the third version, is proposed. It has been improved from both the insulation and thermal standpoints, and the main improvements and additional achievements are as follows.

1) The winding loss is reduced by changing the magnetic wire size from AWG 19 to AWG 17.
2) The local electric field is further reduced through fileting corners and edges winding.
3) The cooling is improved by adding an 8-mm air duct between the winding and the core.
4) The inductor is fully tested in the single-phase full rating tests considering the long-term operation (1 h), validating both the insulation design and thermal design.
5) The repeatability of the design and construction procedure is validated in the building process of another two inductors and the three-phase converter full rating test.

The rest of this article is organized as follows. First, the converter parameters and inductor design requirements are introduced in Section II. Then, the inductor insulation design is discussed in Section III. The physical building of the inductor is introduced in Section IV, and then the insulation test and operational tests are carried out in Sections V and VI, respectively. Finally, Section VII provides the conclusion.

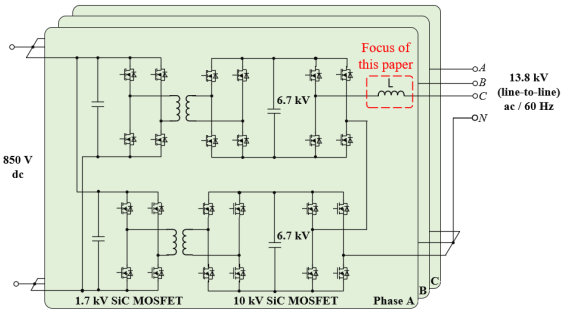

Fig. 1. PCS converter topology.

II. Converter Parameters and Inductor Design Requirements

A. Converter Configuration

As shown in Fig. 1, a power conditioning system (PCS) converter is used to connect an 850-V low voltage (LV) dc to the 13.8-kV MV ac grid. The MV dc-links are rated at 6.7- and 10-kV SiC MOSFETs are used, with a switching frequency of 10 kHz. The dc/ac stage has two full bridges cascaded connected. Phase shift PWM modulation is adopted to generate five-level voltages, and the equivalent switching frequency of the ac side is 40 kHz, so the inductor has current ripples of 40 kHz.

B. Inductor Design Requirements

The inductance is 44 mH, which is mainly determined by the grid-side current harmonic requirement. The inductor needs to have an inrush current capability of 23 A (330% of rated current peak), considering the abnormal grid conditions.

During the steady-state operation, the inductor needs to withstand the total dc-link voltage, which will be around 14 kV considering the dc-link voltage ripples, so the PD inception voltage should be at least 10-kV rms to avoid PD and corresponding insulation capability degradation. Also, according to IEC 60071-1 (2006) [2], the insulation requirements for equipment in the 13.8-kV grid are 95 kV for the rated lightning impulse withstand voltage and 31-kV rms for the rated short-duration (1 min) power frequency withstand voltage. The main converter parameters and inductor design requirements are shown in Table I.

C. Inductor Design Procedure

Considering the inductor high-frequency current ripples, the amorphous core is used, which has higher saturation flux density than ferrite, much smaller core loss than silicon steel, and cheaper than nanocrystalline. The inductor design follows the same design procedure as commonly used filter inductors, as shown in Fig. 2. The winding current density, maximum flux density, and window fill factor are the three variables, and they are determined by iterations to meet the inductor design requirements. In this article, the main focus is the insulation design.

TABLE I
CONVERTER PARAMETERS AND INDUCTOR DESIGN REQUIREMENTS

Converter parameters	LV dc grid voltage	850 V
	MV ac grid voltage	13.8 kV
	Power rating	100 kW
	MV dc-link voltage	6.7 kV
	Switching frequency	10 kHz
Inductor design requirements	Inductance	44 mH
	RMS current	4.2 A
	Inrush current	23 A
	Frequency of dominated current ripple	40 kHz
	Temperature rise	90 ºC
	Cooling approach	Natural air
	Insulation type	Dry type
	PD inception voltage	>10 kV RMS
	Short-duration (1 minute) power frequency withstand voltage	31 kV RMS
	Lightning impulse withstand voltage	95 kV

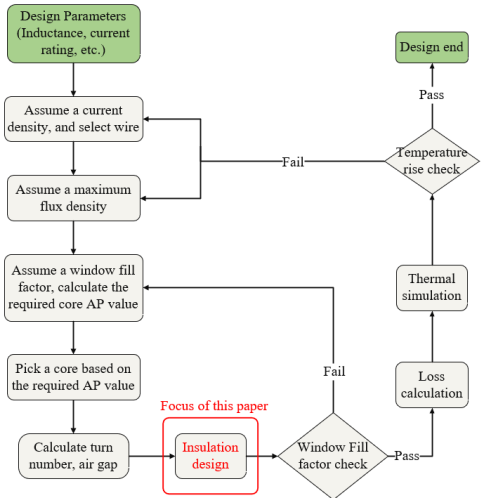

Fig. 2. Inductor design procedure.

TABLE II
INDUCTOR BASIC DESIGN RESULTS

Core material	Amorphous
Core size	AMCC0500
Winding turns	330
Wire gauge	AWG 17
Air gap	5.0 mm
Core loss	18 W
Winding loss	35 W

III. INDUCTOR DESIGN

A. Basic Design Results

Following the design procedure, the inductor basic design results are shown in Table II. The 5.0-mm air gap is divided into two 2.5-mm air gaps at two core legs. The core loss is calculated using the iGSE method [11], and the winding loss includes both the dc resistance and ac resistance losses [12]. The air gap loss is neglected since the distance between the winding and the air gap is much larger than the air gap itself.

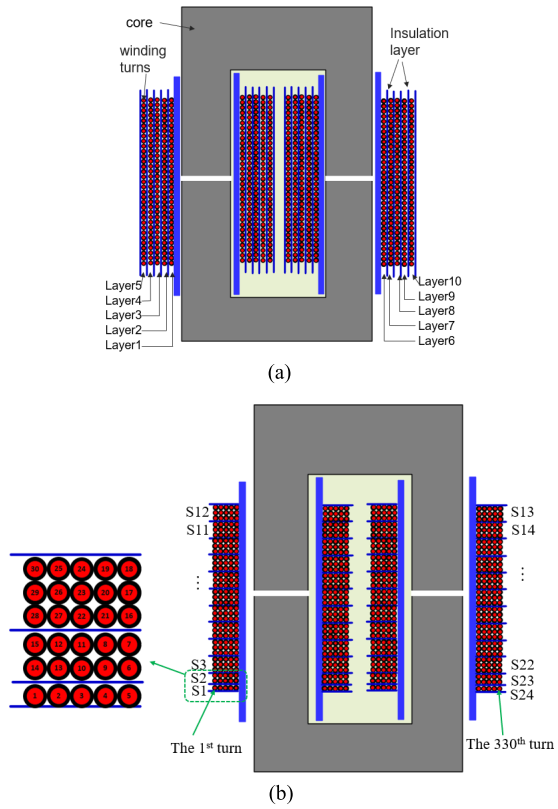

Fig. 3. (a) Commonly used and (b) designed inductor winding structure.

B. Turn-to-Turn and Layer-to-Layer Insulation

In the normal operation, the maximum inductor withstand voltage between its two terminals equals the PCS converter output PWM voltage minus the grid voltage. The maximum value happens when the grid voltage is 0, and in this case, the inductor withstands the MV dc-link voltage, which is 6.7 kV.

The standard 31-kV rms short-duration test is mainly used to test the reliability of equipment in the 13.8-kV system, considering the grid transients, such as switching transient, resonance, and transformer energizing. As for the standard rated lightning impulse withstand voltage, although arresters are installed, which will clamp the lightning surge voltage at a certain level lower than 95 kV, some margin is essential to avoid insulation failure. Then, the winding insulation design also considers the 95 kV.

Therefore, the inductor winding voltage stress is

$$v_{L\_\max} = \begin{cases} 6.7-\text{kV peak}, & \text{normal operation} \\ 44-\text{kV peak}, & \text{short duration} \\ 95-\text{kV peak}, & \text{lightning impulse.} \end{cases} \quad (1)$$

Based on the basic design, the inductor has 330 turns in total. The winding structure, shown in Fig. 3(a), is commonly

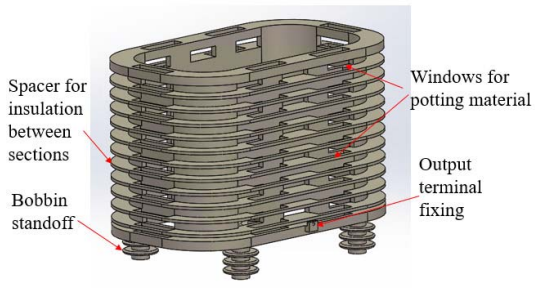

Fig. 4. Designed inductor bobbin.

used in the LV inductor, so it is first considered in the inductor design. Considering the core window area and wire gauge, the 330 turns are divided into ten layers, with 33 turns in each layer, and each core leg has five layers. Although the turn-to-turn insulation requirement is the lowest, which is 1/330 of the inductor voltage stress, the layer-to-layer voltage stress is around 65/330 of the inductor withstand voltage. Assume the inductor voltage is evenly distributed among winding turns, then the layer-to-layer voltage will be 1.32, 8.7, and 18.7 kV during the normal operation, short-duration test, and lightning transient test, respectively. This requires thick insulation layers between winding layers. Therefore, this winding structure is not preferred for this inductor.

To reduce the layer-to-layer voltage stress, a winding structure shown in Fig. 3(b) is designed. Considering the transient voltage distribution due to the parasitic capacitance, the winding turns are unevenly distributed. Section S1 and S24 have five turns per section, S2 and S23 have ten turns per section, and other sections have 15 turns per section. With this structure, although the turn-to-turn voltage stress is increased from 1/330 to 5/330 of the inductor voltage, the layer-to-layer (section-to-section) voltage stress is reduced from 65/330 to 13/330 of the inductor voltage. One advantage of the designed winding structure is that the section spacers can be integrated with the inductor bobbin, and they can be made with insulation material. Another advantage is that this structure contributes to the transient voltage distribution among the winding turns.

The winding bobbin, including the section spacers, can be directly printed out with Formlab's high-temperature 3-D printing material, which has a dielectric strength of 21.6 kV/mm. Considering the strength of the spacer and the wire diameter, the section spacer thickness is determined at 1.4 mm.

The designed inductor bobbin is shown in Fig. 4, the windows cut on the bobbin are used to get the potting material flows into the gaps among wires. The winding terminals will be led out from the middle of the bobbin, and a terminal wire fixing slot has been designed to fix the location of the wire terminal. The bobbin has four standoffs to fix it to the inductor winding case, and the creepage distance between two bobbins on the two core legs along with the standoffs and the inner winding case surface is considered.

C. Winding-to-Core/Ground Insulation

For safety consideration, the inductor core will be grounded. During normal operation, the voltage stress between the

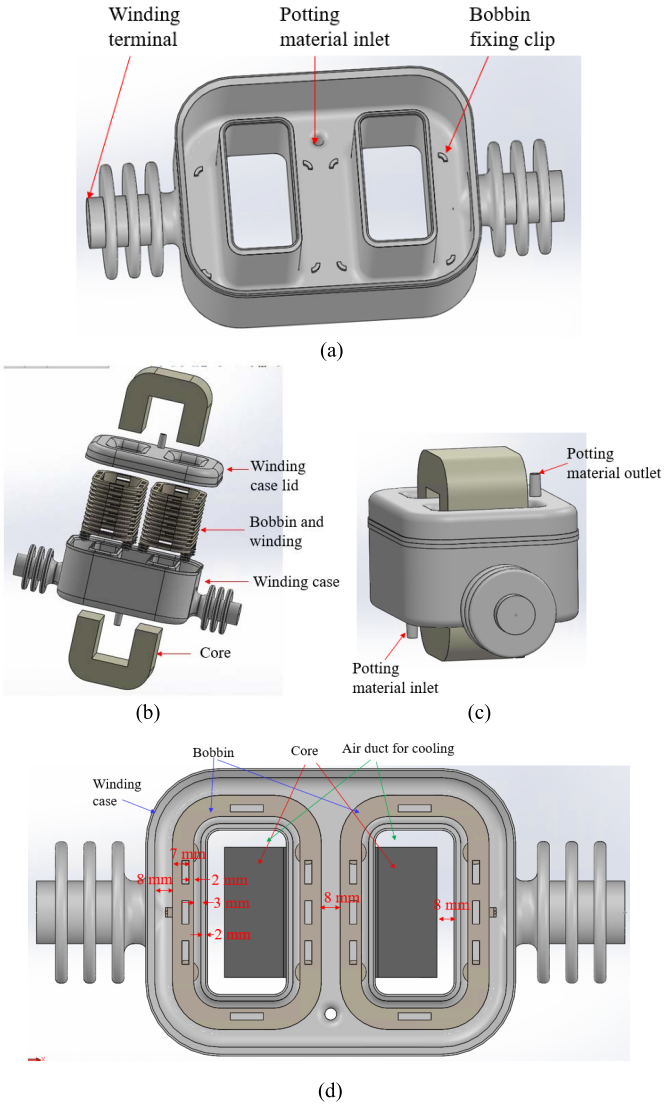

Fig. 5. Inductor winding design of (a) case; (b) assembly of the case, bobbin, lid, and core; (c) inductor after assembled; and (d) insulation distances.

inductor terminal and core (ground) is the total dc-link voltage, which is 13.4 kV. Besides, the 31-kV rms short duration withstands voltage and 95 kV lightning impulse withstand voltage are also considered.

DOWSIL TC 4605 HLV silicone elastomer is selected as the potting material because of its low viscosity (1900 cP), relatively high thermal conductivity (1.0 W/m·K), and high dielectric strength (24 kV/mm). Considering the long-term operation, 7 kV/mm is assumed for the normal operation and short-duration voltage withstand. For the lightning transient, since it is quite short in time, the material insulation capability can be higher. Since no information about the material has been found, a time factor of 0.45 is assumed, referring to the oil [13], which means 15.6 kV/mm of insulation capability is assumed for lightning transient. Therefore, the minimum insulation distance should be

$$d_{\text{insulation}} = \begin{cases} 4.43 \text{ mm}, & \text{normal and short duration} \\ 6.09 \text{ mm}, & \text{lightning.} \end{cases} \quad (2)$$

Then, an inductor winding case is designed, as shown in Fig. 5(a). It is used to contain the winding, ensure the insulation distances, and do contain encapsulants. The creepage distance from the winding terminal to the ground is increased by adding bushing rings on the terminals. A potting material inlet is designed on the container bottom side, and the material outlet is located on the case lid. The case corners and edges are all filleted so that the electric field can be more evenly distributed.

The assembly of the inductor winding case, bobbins, winding case lid, and cores is shown in Fig. 5(b), and the overall inductor structure is shown in Fig. 5(c). To avoid voids and air bubbles, the inductor will be potted with vacuum process, and the potting material will be injected into the winding from the bottom inlet, and the excess material will flow out of the winding from the top outlet.

The insulation distances, bobbin, and case thicknesses are shown in Fig. 5(d). Both the winding case and the bobbins are 3-D printed with materials having similar insulation capability. Since they have similar dielectric strength as the potting material, the thicknesses of the winding case and bobbins can also be treated as insulation distances. Therefore, the insulation distance between the winding and the outer inductor surface is around 8 mm, and the distance from winding to the inner case surface is 7 mm, which are both higher than the requirement shown in (2). The maximum voltage stress between the two winding groups is the total inductor winding voltage, i.e., (1), so the distance between the two winding groups should also meet the requirements in (2). It is designed to be 8 mm, considering some wiring tolerance. Also, an 8 mm air duct between the core and the winding is designed to help dissipate the heat of both the core and the winding.

D. Grounding Shielding

There are air gaps between the core and the winding case, which may result in PD, especially when the temporary or transient overvoltage occurs. To avoid PD in these air gaps, the winding case surface is coated with a thin copper shielding. The shielding layer is grounded together with the cores. This shielding layer creates a constant potential on the winding case surface, and the voltage between the inductor winding and ground is all stressed on the insulation material, i.e., the potting material and the 3-D printing material.

Also, this shielding layer can act as a noise shielding, preventing the EMI noise of the inductor winding from going to the surrounding space.

E. Local Area Electric Field

Although with the shielding layer, the voltage stress is mainly constrained within the insulation materials, it is essential to check the local area electric field to make sure that the maximum electric field does not exceed the material capability.

From the simulation with Ansys/Maxwell, it is found that the terminations are critical areas in terms of the electric field. As shown in Fig. 6, the shielding layer ends at the winding terminal side. Based on the electric field simulation, the electric fields at the terminations of the shielding layer are higher than

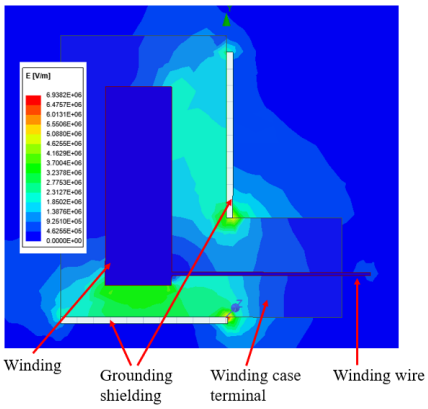

Fig. 6. Local electrical field analysis around the terminal.

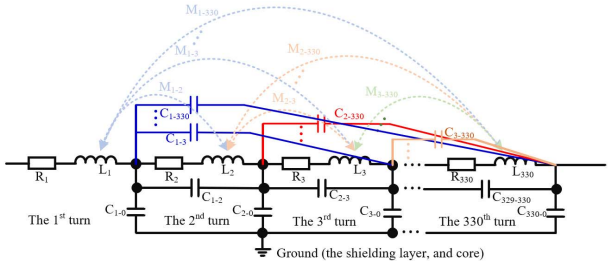

Fig. 7. Equivalent electric circuit of the inductor.

those of other places. Increasing the insulation distance can decrease the local electric field. Finally, the maximum local electric field is controlled to be below 7 kV/mm by increasing the terminal diameter to 30 mm, and the terminal length to 25 mm.

F. Interturn Transient Voltage Analysis

The turn-to-turn insulation is discussed above assuming the voltage stress is evenly distributed among the winding turns, which is true in the steady state. However, during the voltage rising/falling transients, the voltage stress may be unevenly distributed among the winding turns due to the parasitic, and a higher dv/dt will lead to worse uneven distribution. This phenomenon has been widely discussed in the literature, and the most commonly used approach to do analysis is based on the finite element method [14], [15].

An equivalent electric circuit of the inductor is shown in Fig. 7, and each turn of the inductor winding is considered to be an element. Each turn has its resistance and inductance, and mutual inductance between any two turns. Also, there is a parasitic capacitance between any two turns and between the turn and the ground (the shielding layer).

Therefore, three parasitic matrices, C, R, and L for the capacitance, resistance, and inductance, respectively, can be used to express the inductor parasitic

$$\boldsymbol{C} = \begin{bmatrix} \backslash & C_{0-1} & C_{0-2} & \cdots & C_{0-330} \\ C_{1-0} & \backslash & C_{1-2} & \cdots & C_{1-330} \\ C_{2-0} & C_{2-1} & \backslash & \cdots & C_{2-330} \\ \vdots & \vdots & \vdots & \ddots & \vdots \\ C_{330-0} & C_{330-1} & C_{330-2} & \cdots & \backslash \end{bmatrix}$$

$$\boldsymbol{R} = \begin{bmatrix} R_1 & 0 & 0 & \cdots & 0 \\ 0 & R_2 & 0 & \cdots & 0 \\ 0 & 0 & R_3 & \cdots & 0 \\ \vdots & \vdots & \vdots & \ddots & \vdots \\ 0 & 0 & 0 & \cdots & R_{330} \end{bmatrix}$$

$$\boldsymbol{L} = \begin{bmatrix} L_1 & M_{1-2} & M_{1-3} & \cdots & M_{1-330} \\ M_{2-1} & L_2 & M_{2-3} & \cdots & M_{2-330} \\ M_{3-1} & M_{3-2} & L_3 & \cdots & M_{3-330} \\ \vdots & \vdots & \vdots & \ddots & \vdots \\ M_{330-1} & M_{330-2} & M_{330-3} & \cdots & L_{330} \end{bmatrix} \quad (3)$$

where C_{j-k} is the capacitance between node j and k; R_k and L_k are the resistance and inductance of the kth turn, respectively; M_{j-k} is the mutual inductance between the jth turn and kth turn.

The capacitance and inductance matrix values are obtained from the ANSYS MAXWELL electrostatic and magnetostatic simulation, respectively. The resistance is estimated by calculating the ac resistance under the equivalent frequency corresponding to the rise time and falling time of the PWM pulse [14]. After obtaining the parasitic matrix values, an LTspice inductor model is built and used to evaluate the interturn voltage distribution during transients.

The interturn transient voltage waveform comparison at different winding locations is shown in Fig. 8(a). The average dv/dt of the 10-kV SiC MOSFET used in the converter is around 50–60 V/ns, but the transient dv/dt could be up to 100 V/ns. Therefore, 100 V/ns is assumed in the comparison. The PWM voltage applied on the inductor increases from 0 to the dc-link voltage (6.7 kV) within 670 ns. There are two types of interturn voltage in each winding section, of which type-I is the voltage between two adjacent turns and the turn number difference is 1, and type-II is the voltage between two adjacent turns with the maximum turn number difference. During the switching transient, the interturn voltage distribution is uneven, and the interturn voltage close to the converter side is higher than that close to the grid side. The first turn has the highest transient voltage overshoot, which is around 45% of the steady-state voltage. The maximum type-II interturn voltage also occurs at the terminal side (turn 16–turn 21), which is around 130 V. Since the type-II interturn voltage is higher than type-I, it needs to be considered as the maximum turn-to-turn voltage stress and be a consideration in magnetic wire selection.

The interturn voltage uneven distribution is also studied considering different dv/dt conditions. As shown in Fig. 8(b), a higher dv/dt leads to a larger interturn voltage peak. The dv/dt caused by grid-side transients, such as switching or faults, is much smaller than 100 V/ns. The dv/dt caused by lightning is fast, but it is still slower (considering 95 kV/1.2 μs = 79 V/ns) than 100 V/ns, so the voltage uneven distribution will be better than that in the PWM switching transients.

G. Thermal Simulation

To check the inductor thermal performance, the thermal simulation is conducted with Ansys/Icepak after the insulation design.

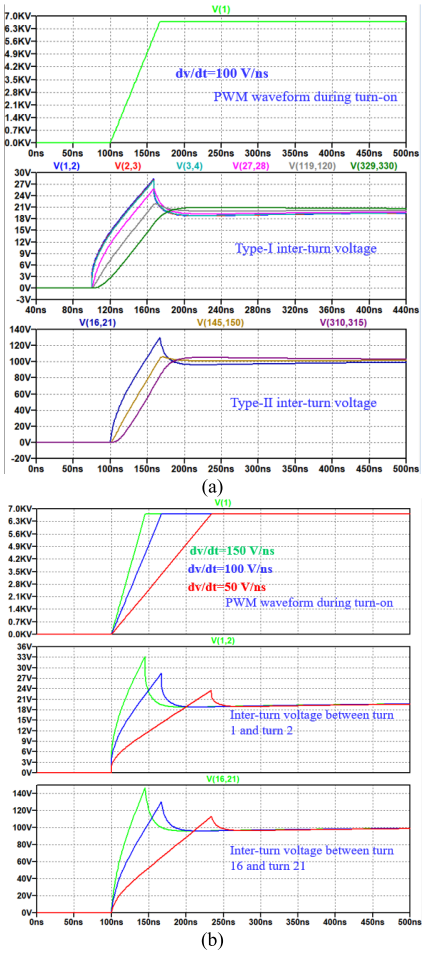

Fig. 8. Interturn transient voltage distribution waveforms considering (a) different locations with dv/dt = 100 V/ns; (b) different dv/dt (green: 150 V/ns; blue: 100 V/ns; and red: 50 V/ns).

From the cross-sectional temperature distribution, as shown in Fig. 9(a), it can be found that the hot spot locates in the inner winding inside the core window, and the temperature rise is around 58 °C (the ambient is 20 °C in the simulation). The hot spot on the surface locates on the top center of the winding, as shown in Fig. 9(b), and the maximum temperature rise is around 52 °C. This temperature distribution is because the winding in the core window has a higher loss but less efficient heat dissipation than the winding parts at the left and right sides. The heat dissipation of the winding in the core window is more difficult due to the thermal interference between the core and the winding and less exposed surface area to the air. Although the temperature rise is lower than the requirement, which is 90 °C, considering the uneven loss distribution and loss calculation tolerance, some margin is necessary. Fig. 9(c) shows the air velocity surrounding the inductor, with natural-air cooling, the air velocity in the winding air duct is around 0.3 m/s, which helps to dissipate the heat of both the winding and the core.

IV. Inductor Physical Building

A. Winding Building

MWS heavy polyimide NEMA MW16-C magnetic wire is used to build the winding. It has a temperature rating of

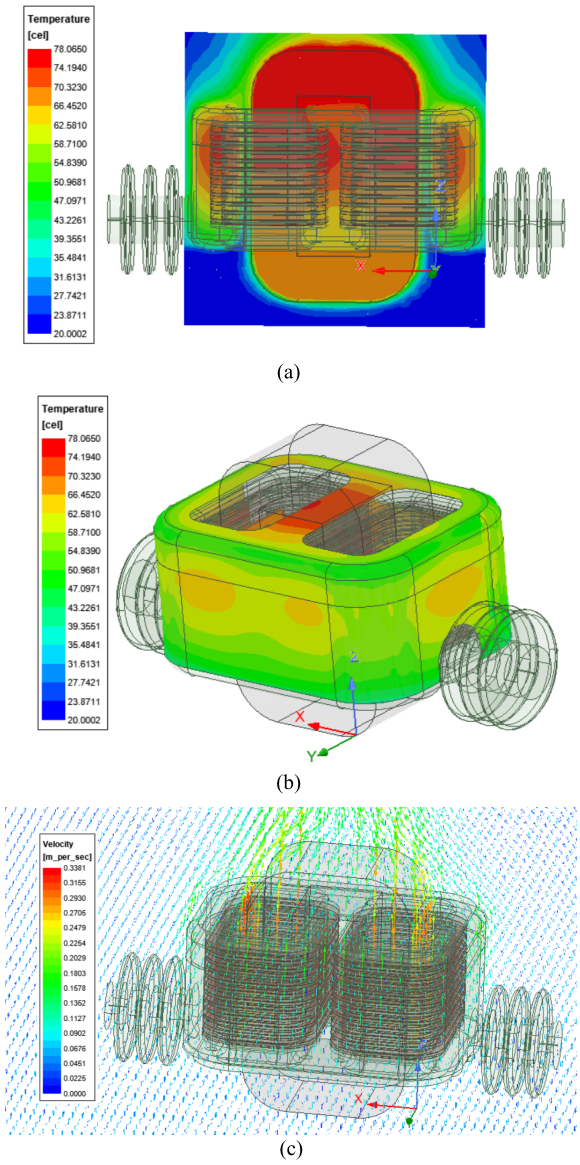

Fig. 9. Inductor thermal simulation results. (a) Cross-sectional temperature distribution. (b) Surface temperature distribution. (c) Air velocity.

240 °C, a dielectric breakdown voltage of 5.85 kV, and a continuous peak operating voltage of up to 1.1 kV. It can meet the interturn insulation requirements considering both the steady-state and transient conditions. As shown in Fig. 10(a), the inductor winding is wound on two bobbins. The winding case and case lid are shown in Fig. 10(b) and (c), respectively. The assembly of the winding and the winding case is shown in Fig. 10(d). The magnetic wire directly led out from the winding case terminals.

B. Winding Potting

The inductor lid and case are sealed with epoxy first to avoid leakage during the potting process. Then, the inductor is potted in the setup shown in Fig. 11(a), and the setup diagram is shown in Fig. 11(b), referring to the setup in [6].

The setup consists of an air tube and a material tube. The air tube connects two vacuum chambers to the vacuum pump,

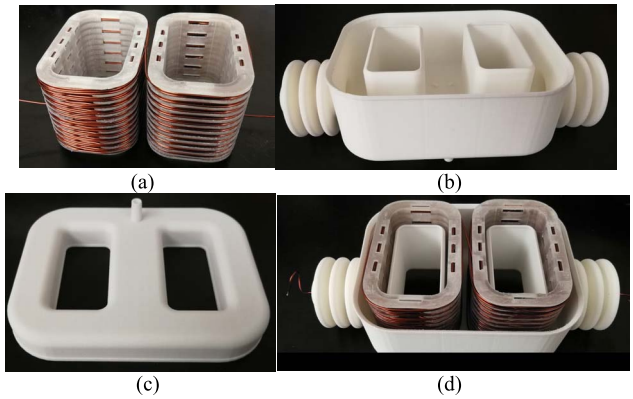

Fig. 10. Winding building (a) winding; (b) winding case; (c) winding case lid; and (d) assembly of the winding and the case.

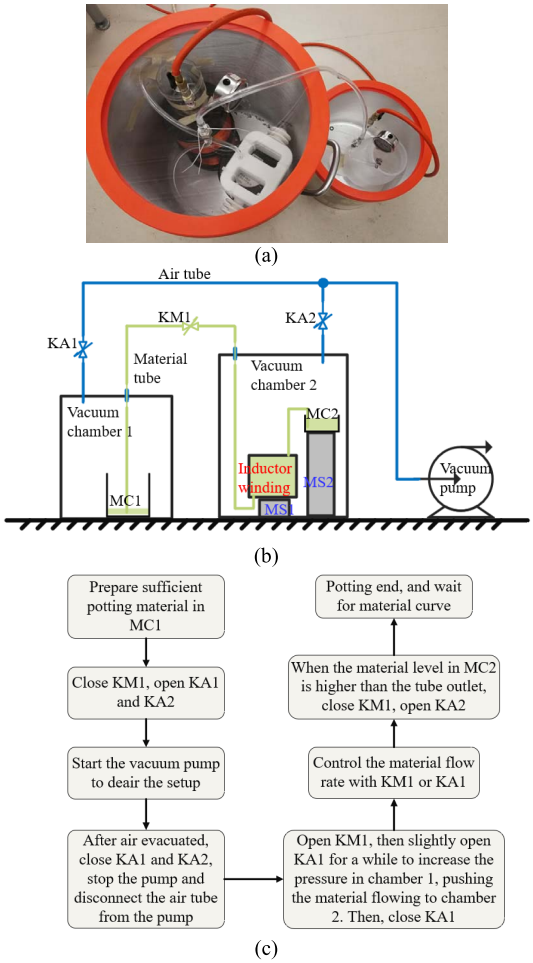

Fig. 11. Inductor potting. (a) Setup hardware. (b) Setup diagram. (c) Procedure.

and two valves, KA1 and KA2 are installed on each chamber's air tube, respectively. The material tube connects from the material container, MC1, in the vacuum chamber 1 to the inlet of the inductor winding in the vacuum chamber 2. There is a material valve, KM1, which can be used to control the material flow rate. The inductor potting material outlet is connected to another material container, MC2, which is located at a higher location than the inductor winding. The potting procedure is shown in Fig. 11(c).

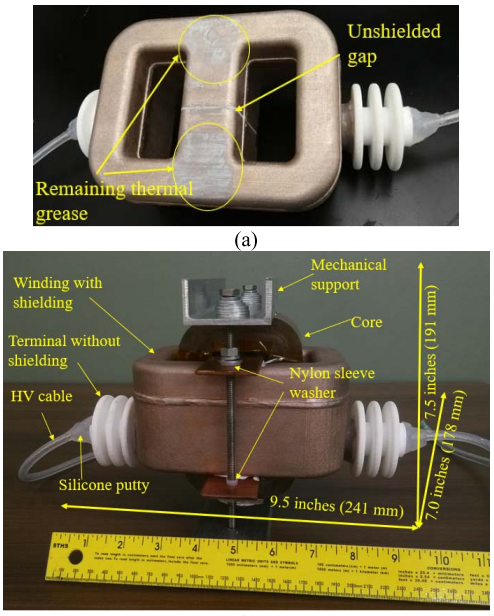

Fig. 12. Photographs of (a) inductor winding with shielding and (b) inductor after assembly.

C. Winding Shielding and Inductor Assembly

After the potting material is fully cured, the shielding layer is applied to the surface of the inductor winding. 843WB liquid electromagnetic shielding paint, which has a resistivity of 5.3×10^{-4} Ω·cm, is used as the shielding material. It needs to be mentioned that an unshielded gap on the center leg of the inductor winding needs to be kept, as shown in Fig. 12(a). Otherwise, the conductive shielding layer will form two turns surrounding the two core legs respectively, which leads to loss and generates heat and will damage the shielding layer or even the inductor insulation. To avoid the negative impact of the mechanical fixing items (copper bars) on the winding heat dissipation, a thin layer of thermal grease will be applied to fill the gap between the winding surface and the copper bar. Before applying the thermal grease, a piece of Kapton tape is applied over the unshielded gap, to avoid the short circuit through thermal grease. A thin layer of Kapton tape is also applied to the copper bars to avoid the short circuit through them.

The inductor assembly is shown in Fig. 12(b). The shielding layer is only applied on the main winding body but not applied on the two terminals to leave sufficient creepage distance. Also, HV cables are used to connect the magnetic wire terminals, and 10-8880 HV silicone putty is used to seal the soldering junction to avoid creepage discharge. The winding and two cores are fixed with metal screws, copper bars, and aluminum U-channels, and they are all connected and then grounded. Two electrical insulating nylon 6/6 sleeve washers, which have a thickness of 1.6 mm, are used at one side of the screw to avoid forming another turn surrounding the core; otherwise, it will also induce losses.

The dimension of the inductor, including the mechanical structure and two terminals, is $9.5 \times 7.0 \times 7.5$ in^3 ($24.1 \times 17.8 \times 19.1$ cm^3), and the weight is 12.6 lbs (5.7 kg). The inductor weight breakdown is shown in Fig. 13, and the core, potting material, and the magnetic wire are the three main parts, occupying 51%, 15%, and 15%, respectively.

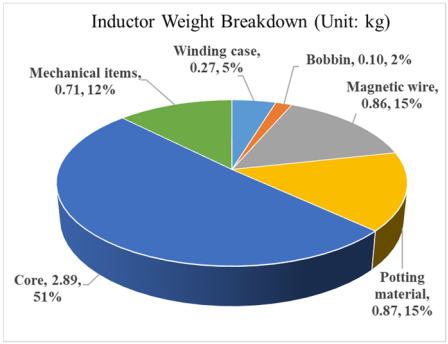

Fig. 13. Inductor weight breakdown.

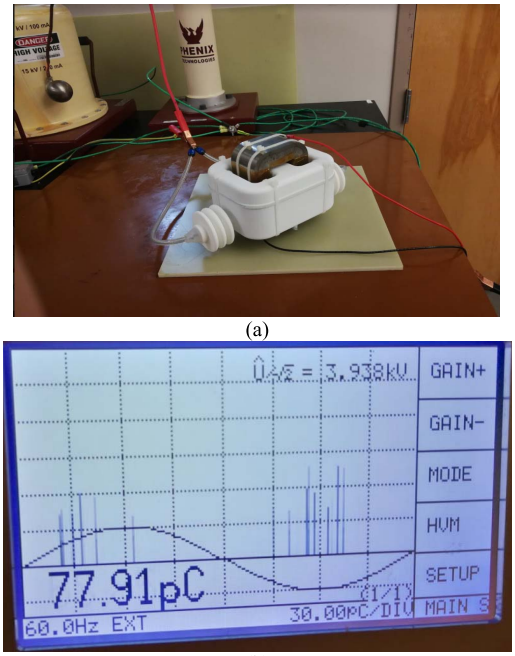

Fig. 14. PD test of the inductor without the shielding layer. (a) Test setup. (b) PD waveform.

V. Insulation Tests

A. PD Test

To verify the shielding layer design, the PD test is conducted first without the shielding layer. The PHENIX PD tester 6CP30/15-3 is used. As shown in Fig. 14(a), the positive terminal of the PD tester is connected to the two inductor terminals, and the ground terminal is connected to the core. The PD occurs at around 3.4 kV rms, and the PD level is around 78 pC when the voltage increased to 3.938-kV rms, as shown in Fig. 14(b).

After the shielding has been applied, the inductor has been fully assembled and then tested with the same PD tester. As shown in Fig. 15(a), the PD tester positive terminal is also connected to the two inductor terminals, and the

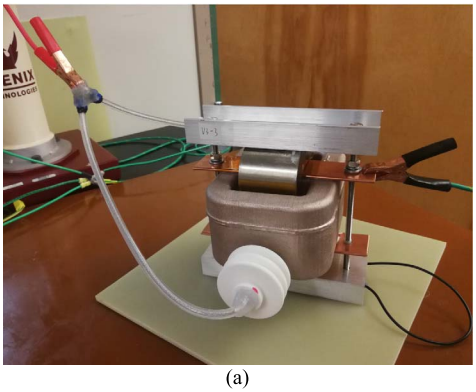

(a)

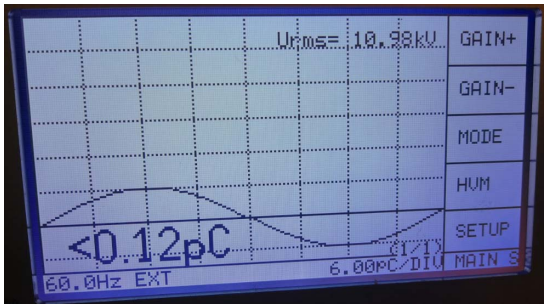

(b)

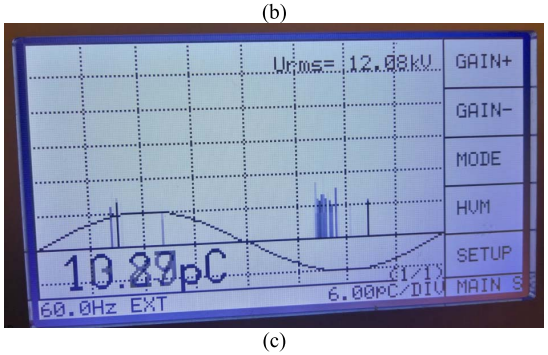

(c)

Fig. 15. PD test of the inductor with the shielding layer. (a) Test setup. (b) PD waveform at 10.98-kV rms. (c) PD waveform at 12.08-kV rms.

ground terminal is connected to the inductor mechanical frame, which is also connected to the core and shielding layer. Fig. 15(b) and (c) show the PD test results at 10.98 and 12.08 kV, respectively. It can be found that at 10.98-kV rms, there is no PD, and the PD value is around 13 pC at 12.08-kV rms. According to IEEE Std C57.12.01 (2020) [16], the maximum acceptable level of PD for solid cast winding is 10 pC and for resin-encapsulated winding is 50 pC. This inductor belongs to the second type, and it has a PD capability of higher than 12.1 kV.

Through the PD test comparison without and with the shielding layer, the shielding concept has been validated, and it helps the inductor to have a better PD performance.

B. Hi-Pot Test

The dc hi-pot test is then carried out with PHENIX 4100-10 dc hi-pot tester, and the hi-pot voltage is applied between the winding terminals and the shielding layer.

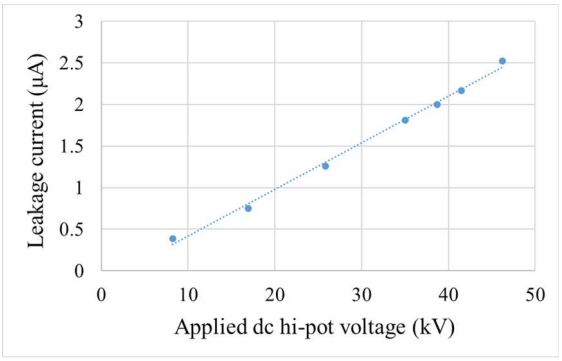

Fig. 16. DC hi-pot test results.

The applied hi-pot test voltage is gradually increased from 0 to 46 kV, which is higher than the peak value of the 31-kV rms short-duration (1 min) power frequency withstand voltage. No breakdown has been observed during the testing process. The leakage currents read from the hi-pot tester at some voltage levels have been recorded, and at each recorded voltage level, the testing has been conducted for more than one minute.

The dc hi-pot test results are shown in Fig. 16. It can be found that the leakage current linearly increases with the applied hi-pot voltage, which means the insulation between the winding and the shielding layer is mainly high resistive and the impedance is around 20 GΩ.

VI. Operational Tests

A. Single-Phase Full Rating Test

The inductor has been tested in the single-phase PCS converter first. The test setup diagram is shown in Fig. 17(a), and the hardware picture is shown in Fig. 17(b). The PCS converter is supplied from the LV dc side with an LV dc power supply. At the MV ac side, a 60 Hz, 8 kV to 120 V transformer is used, and a 0.42 Ω/45 kW resistive load is connected at the LV ac side. To avoid high core loss due to the high switching frequency ripple, a capacitor is used to form an *LC* filter and filter out the high switching frequency ripples for the 60-Hz transformer.

The MV ac side voltage and current waveforms are shown in Fig. 17(c). The PWM waveforms have five levels, and the second-order voltage ripple caused by the single-phase power variation can be observed from the PWM waveform outline. With the *LC* filter, the ac voltage and current waveforms are sinusoidal, and their rms values are 7.81 kV and 4.27 A, respectively, and the output power is 33.3 kW.

To verify the insulation design in long-term operation, the inductor was tested under the full rating for 1 hour. No abnormal phenomena, such as electrical breakdown or odor, have been found.

Moreover, insulation performance is highly related to thermal performance. The insulation issue will induce additional loss and then cause a thermal issue. Therefore, the thermal performance of the inductor during the long-term test is an

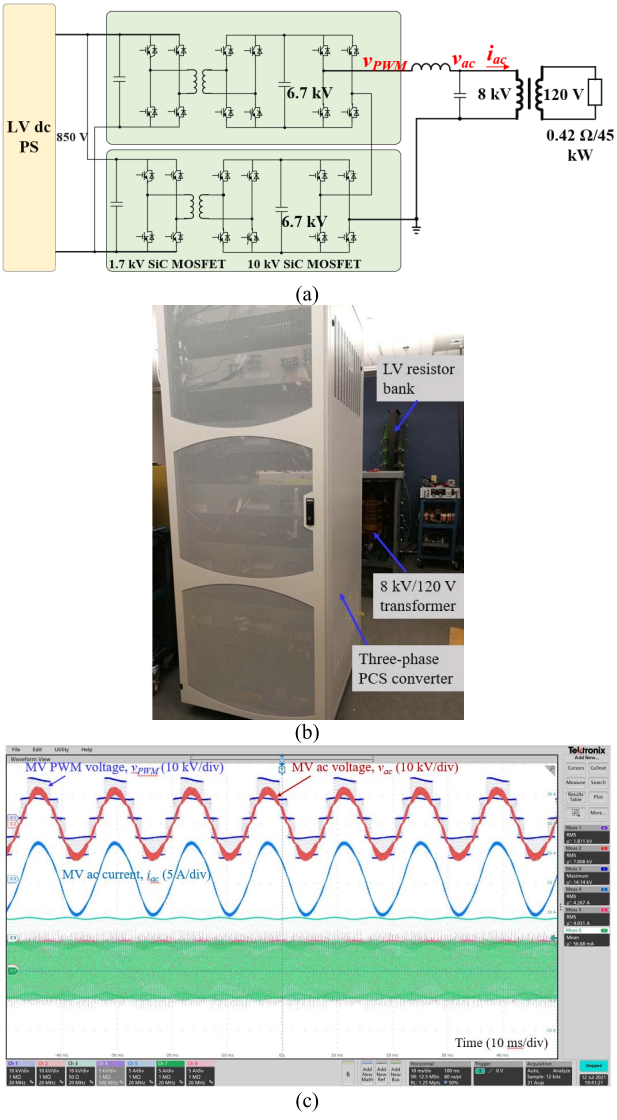

Fig. 17. Single-phase test at the rated voltage and power rating. (a) Test setup. (b) Setup photograph. (c) AC voltage and current waveforms.

important indicator of the insulation performance. During the test, four fiber optic temperature sensors are used to measure the inductor temperatures at four different locations. Two of them are applied on the surface of the core at the front side and in the air gap, respectively. The other two are applied on the winding surfaces at the front area and the top area, respectively.

The thermal image of the inductor taken after 1-hour operation is shown in Fig. 18(a). It can be found that the hot spot is in the gap between the core and the winding. The maximum temperature is around 88 °C, so the temperature rise is around 66 °C, considering 22 °C of ambient temperature.

The core and winding temperature curves are shown in Fig. 18(b). Although the inductor does not reach its thermal equilibrium, curve fittings are carried out to extend the measured temperature curves to their steady state, by treating the inductor thermal response to be an *RC* network [17]. Based on the curve fitting, it takes around 2.5 and 5 h for the inductor

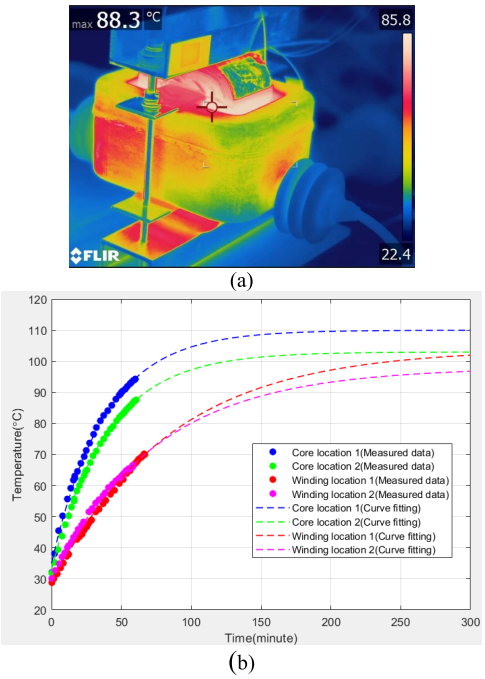

Fig. 18. Inductor thermal performance after 1-h continuous operation at the rated voltage and power rating. (a) Thermal image. (b) Temperature curves.

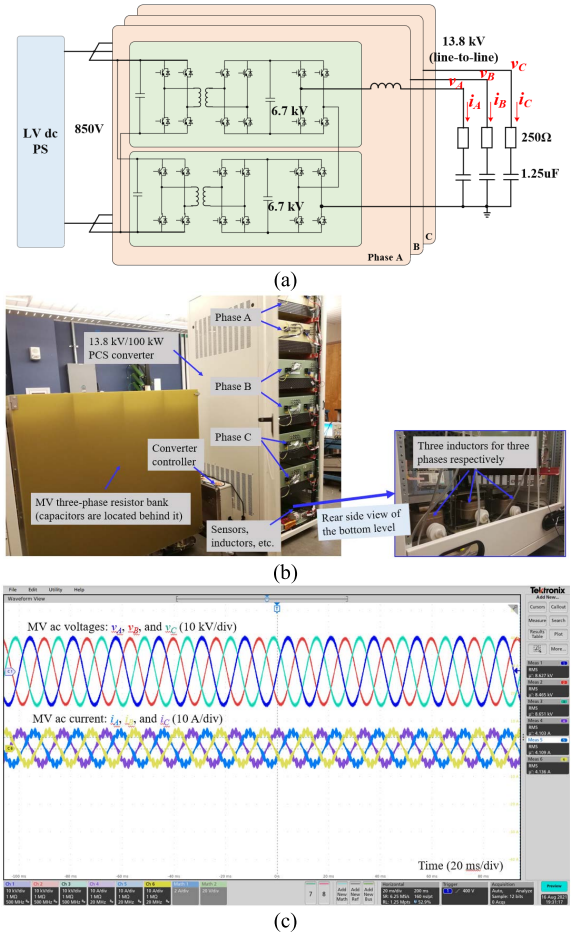

Fig. 19. Three-phase test at the rated voltage and power rating. (a) Test setup. (b) Test setup photograph. (c) AC voltage and current waveforms.

core and winding to get to the thermal equilibrium. In the thermal equilibrium, the maximum core temperature will be

around 110 °C, and the winding temperature will be around 104 °C, which means the maximum temperature rise is around 88 °C (considering 22 °C of ambient temperature). Although the temperature rise is higher than the thermal simulation, the difference is acceptable considering the loss estimation error and uneven distribution.

B. Three-Phase Full Rating Test

Then, another two inductors are built following the same design; they have similar PD test results as the first one. The three inductors are tested in the three-phase 13.8 kV/100 kV·A PCS converter. The test setup and hardware picture are shown in Fig. 19(a) and (b), respectively. *RC* loads are connected at the MV ac side to consume 100 kV·A so that the ac side is tested under the rated condition. The MV ac voltage and current waveforms are shown in Fig. 19(c), and the ac line-to-line voltage is around 14.7 kV, and the output power is 106 kV·A. All three inductors work well in the test, and no issue was found.

Therefore, with single-phase tests and three-phase tests, the inductor insulation design is further validated.

VII. Conclusion

This article discussed the insulation design of the filter inductor in a 13.8-kV grid-connected PCS converter. Besides the normal operation, the short-duration (1 min) power frequency withstand voltage and the lightning impulse voltage required in IEC 60071-1 (2006) are considered. The inductor winding bobbins are designed to reduce the voltage stress between turn to turn and section to section. A winding case is designed to contain the bobbins and ensure the insulation distance between the winding and the ground.

To avoid PD in the air gap between the winding and the core and reduce the inductor size, a conductive shielding layer has been applied on the surface of the winding case, which can constrain the electric field within the insulation material. Also, the shielding layer can help reduce the EMI noise of the inductor since it is grounded.

The shielding layer design is validated through PD test comparison between without and with the shielding layer. The 12-kV PD test, 46 kV (>1 min) dc hi-pot test, 13.8 kV/33.3 kW 1-h single-phase test, and 13.8 kV/100 kVA three-phase test validated the inductor design.

Acknowledgment

The authors would like to thank the contribution of Southern Company, Birmingham, AL, USA, and Powerex, Youngwood, PA, USA.

References

[1] J. Thoma, B. Volzer, D. Kranzer, D. Derix, and A. Hensel, "Design and commissioning of a 10 kV three-phase transformerless inverter with 15 kV silicon carbide MOSFETs," in *Proc. 20th Eur. Conf. Power Electron. Appl. (EPE ECCE)*, 2018, pp. P.1–P.7.

[2] *Insulation Co-Ordination—Part 1: Definitions, Principles and Rules*, Standard IEC 60071-1, 2006.

[3] S. Madhusoodhanan *et al.*, "Solid-state transformer and MV grid tie applications enabled by 15 kV SiC IGBTs and 10 kV SiC MOSFETs based multilevel converters," *IEEE Trans. Ind. Appl.*, vol. 51, no. 4, pp. 3343–3360, Jul./Aug. 2015.

[4] X. She, X. Yu, F. Wang, and A. Q. Huang, "Design and demonstration of a 3.6-kV-120-V/10-kVA solid-state transformer for smart grid application," *IEEE Trans. Power Electron.*, vol. 29, no. 8, pp. 3982–3996, Aug. 2014.

[5] H. Zhao *et al.*, "Physics-based modeling of parasitic capacitance in medium-voltage filter inductors," *IEEE Trans. Power Electron.*, vol. 36, no. 1, pp. 829–843, Jan. 2021.

[6] D. Rothmund, T. Guillod, D. Bortis, and J. W. Kolar, "99% efficient 10 kV SiC-based 7 kV/400 V DC transformer for future data centers," *IEEE J. Emerg. Sel. Topics Power Electron.*, vol. 7, no. 2, pp. 753–767, Jun. 2019.

[7] M. Kaymak, R. W. De Doncker, and T. Jimichi, "Design and verification of a medium-frequency transformer in a three-phase dual-active bridge DC–DC converter for medium-voltage grid connection of offshore wind farms," in *Proc. IEEE Appl. Power Electron. Conf. Expo. (APEC)*, Mar. 2020, pp. 2694–2701.

[8] T. B. Gradinger, U. Drofenik, and S. Alvarez, "Novel insulation concept for an MV dry-cast medium-frequency transformer," in *Proc. 19th Eur. Conf. Power Electron. Appl. (EPE ECCE)*, Sep. 2017, pp. P.1–P.10.

[9] Q. Chen, R. Raju, D. Dong, and M. Agamy, "High frequency transformer insulation in medium voltage SiC enabled air-cooled solid-state transformers," in *Proc. IEEE Energy Convers. Congr. Expo. (ECCE)*, Sep. 2018, pp. 2436–2443.

[10] H. Li, P. Yao, Z. Gao, and F. Wang, "Medium voltage converter inductor insulation design considering grid insulation requirements," in *Proc. IEEE Appl. Power Electron. Conf. Expo. (APEC)*, Jun. 2021, pp. 2120–2126.

[11] K. Venkatachalam, C. R. Sullivan, T. Abdallah, and H. Tacca, "Accurate prediction of ferrite core loss with nonsinusoidal waveforms using only steinmetz parameters," in *Proc. IEEE Workshop Comput. Power Electron.*, Jun. 2002, pp. 36–41.

[12] A. Reatti and M. K. Kazimierczuk, "Comparison of various methods for calculating the AC resistance of inductors," *IEEE Trans. Magn.*, vol. 38, no. 3, pp. 1512–1518, May 2002.

[13] A. Küchler, *High Voltage Engineering: Fundamentals-Technology-Applications*. Berlin, Germany: Springer, 2017, pp. 236–237.

[14] F. Wen, L. Zhang, G. Wu, and E. He, "Modeling and simulation of inter-turn voltage distribution in the stator windings of the pulling motor," in *Proc. IEEE Int. Conf. Solid Dielectr. (ICSD)*, Jul. 2004, pp. 900–903.

[15] C. Zheng, Q. Wang, H. Wang, C. L. Bak, and Z. Shen, "Uneven inter-turn voltage distribution among windings of medium-voltage medium/high-frequency transformers," in *Proc. IEEE Int. Conf. High Voltage Eng. Appl. (ICHVE)*, Sep. 2020, pp. 1–4.

[16] *IEEE Standard for General Requirements for Dry-Type Distribution and Power Transformers*, IEEE Standard C57.12.01-2020 (Revision of IEEE Standard C57.12.01-2015), 2020, pp. 1–49.

[17] H. Tian, Z. Wei, M. P. Thevar, S. Vaisambhayana, A. Tripathi, and P. C. Kjaer, "Experimental verification on thermal modeling of medium frequency transformers," in *Proc. 44th Annu. Conf. IEEE Ind. Electron. Soc. (IECON)*, Oct. 2018, pp. 5527–5534.

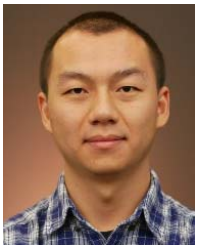

Haiguo Li (Graduate Student Member, IEEE) received the B.S. and M.S. degrees in electrical engineering from Shanghai Jiao Tong University, Shanghai, China, in 2014 and 2017, respectively. He is currently pursuing the Ph.D. degree with The University of Tennessee, Knoxville, Knoxville, TN, USA.

His research interests include grid-connected converter design, control, and test, medium voltage (MV) SiC device application in grid power electronics, MV converter design and control, and MV gate driver power supply.

Pengfei Yao (Member, IEEE) was born in Inner Mongolia, China, in 1992. He received the B.S. and Ph.D. degrees in electrical engineering from Tsinghua University, Beijing, China, in 2015 and 2020 respectively.

From 2019 to 2020, he was a Visiting Scholar with CURENT, The University of Tennessee, Knoxville, Knoxville, TN, USA. He is currently with the China Huaneng Group, Beijing. His research interests include offshore wind power generation, grid integration of multiple energy including renewable energy, and design and control of grid connected high power isolated dc–dc converters.

Zihan Gao (Student Member, IEEE) received the B.S. degree in electrical engineering from Huazhong University of Science and Technology, Wuhan, China, in 2018. He is currently pursuing the Ph.D. degree with The University of Tennessee, Knoxville, Knoxville, TN, USA.

He is currently a Graduate Research Assistant with the Center for Ultra-Wide-Area Resilient Electric Energy Transmission Networks (CURENT), Department of Electrical Engineering and Computer Science, The University of Tennessee, Knoxville. His research interests include medium voltage (MV) dc/dc converters and MV medium frequency transformers.

Fei (Fred) Wang (Fellow, IEEE) received the B.S. degree in electrical engineering from Xi'an Jiaotong University, Xi'an, China, in 1982, and the M.S. and Ph.D. degrees in electrical engineering from the University of Southern California, Los Angeles, CA, USA, in 1985 and 1990, respectively.

He was a Research Scientist with the Electric Power Laboratory, University of Southern California, from 1990 to 1992. He joined the GE Power Systems Engineering Department, Schenectady, NY, USA, as an Application Engineer, in 1992. From 1994 to 2000, he was a Senior Product Development Engineer with GE Industrial Systems, Salem, VA, USA. From 2000 to 2001, he was the Manager of Electronic & Photonic Systems Technology Laboratory, GE Global Research Center, Schenectady and Shanghai, China. In 2001, he joined the Center for Power Electronics Systems (CPES), Virginia Tech, Blacksburg, VA, USA, as a Research Associate Professor and became an Associate Professor in 2004. From 2003 to 2009, he also served as the CPES Technical Director. Since 2009, he has been with The University of Tennessee, Knoxville and Oak Ridge National Laboratory, Knoxville, TN, as a Professor and the Condra Chair of Excellence in Power Electronics. He is a Founding Member and the Technical Director of the multiuniversity NSF/DOE Engineering Research Center for Ultra-wide-area Resilient Electric Energy Transmission Networks (CURENT) led by The University of Tennessee, Knoxville. His research interests include power electronics and power systems.

Dr. Wang is a fellow of the U.S. National Academy of Inventors.